Fault Diagnostic Device for Photovoltaic Panels

Wenguan Wang[1,2], Alex Chun-for Liu[1], Henry Shu-hung Chung[1],
Ricky Wing-hong Lau[1], Jun Zhang[2], and Alan Wai-lun Lo[3]

[1] Centre for Smart Energy
Conversion and Utilization Research
City University of Hong Kong
Kowloon Tong, Hong Kong

[2] Department of Computer Science
Sun Yat-sen University
Guangzhou, Guangdong
People's Republic of China

[3] Department of Computer Science
Chu Hai College of Higher Education
Yi Lok Street, Riviera Garden,
Tsuen Wan, Hong Kong.

***Abstract* – A device for fault diagnosis of photovoltaic (PV) panels is presented. By sampling the terminal voltage and current of the panel when the connected PV system is tracking the maximum power point, the device simultaneously utilizes the sampled information to estimate and observe the drift of the intrinsic parameters of the panel. Compared with prior-art approaches of using static current–voltage characteristics to perform fault diagnosis, the proposed device extracts the dynamic characteristics, allowing fast parameter estimation and offering an in-depth understanding of the failure mode. A prototype device has been built and evaluated on a test bed with four 80W panels, with two of them being healthy and the other two having different degrees of damage. All experiments are conducted under a controlled testing environment. Results reveal that the intrinsic parameters, such as the reverse saturation current, output resistance, and junction capacitance, of the damaged panels can significantly deviated from the nominal values. This gives an indication of the health of the panel. Moreover, the prototype sends the estimated intrinsic parameters to the PV system over the power cable through power line communication. Therefore, the merits of this concept lie in its modularity, scalability, and remote fault diagnosis capability.**

Keywords – Photovoltaic systems, reliability, fault diagnosis, solar panels

I. INTRODUCTION

Photovoltaic (PV) energy is being widely used in today's environmentally-conscious world. As the power generation of PV systems depends on many environmental conditions, such as insolation level and ambient temperature, the last four decades have witnessed a great deal of research effort devoted to advancing the materials for improving cell efficiency and the system architecture for extracting more power from the solar cells. In order to increase system reliability, fault diagnosis of PV panels is equally important, as the lifetime of the PV panels is typically longer than 20 years. There are many prior-art fault detection methods and classification models for PV modules [1]-[9]. They are mainly based on using the static current-voltage (I-V) characteristics of the panels to diagnose the condition of the panel under different environmental conditions. Such static I-V characteristics are typically obtained by sweeping the terminal voltage or current of the panel. However, due to the presence of the junction capacitance associated with the panel [5], the dynamic I-V characteristic would deviate from the static I-V characteristic significantly if a fast sweeping process is taken. Fig. 1 shows the static I-V characteristic and dynamic I-V characteristics under different sweeping frequencies. The discrepancy between the static and dynamic I-V characteristics increases as the sweeping frequency increases. It is mainly because the junction capacitance introduces an AC current at the terminal during the sweeping process. A feasible way to get the static I-V characteristic is to sweep the terminal voltage and current slowly. Conventional models [1]-[3] obtain a high-precision static I-V characteristic by shedding the load for some time or conduct the measurement offline. However, this will cause undesired interruption to the power generation by the PV panels. Thus, in order to speed up the process of determining the static I-V characteristics, it is necessary to take the effect of the junction capacitance on affecting the dynamic I-V characteristic into account in extracting the intrinsic parameters [5].

Extraction of intrinsic parameters of PV panels is a black-box problem or problem without known derivative, because only the terminal voltage and current can be measured. Among different parameter extraction techniques, computational intelligence (CI), which is a set of nature-inspired computational algorithms, is applicable for tackling this kind of problems. In [6]-[8], a CI algorithm is used to locate the maximum power point (MPP) of PV panels, but not extract intrinsic parameters. In [10], a particle swarm optimization (PSO) technique is used to extract intrinsic parameters, but the junction capacitance of the panel has not been taken into account.

A fault diagnostic device (FDD) that utilizes the measured voltage and current information, when the PV system is locating the MPP, to conduct real-time intrinsic parameter estimation is presented. No explicit sweeping process is needed. This diagnosing method allows minimum interruption to the PV power generation. The estimation algorithm is based on a modified (PSO) technique that can avoid trapping into local optima. The technique has been applied to a prototype device using a Cortex M4 microcontroller unit. Moreover, the proposed diagnostic device has the power line communication (PLC) function, so the intrinsic parameters can be sent back to the central control unit through the power cables connecting between the PV system and panels.

978-1-4799-6735-3/15/$31.00 ©2015 IEEE

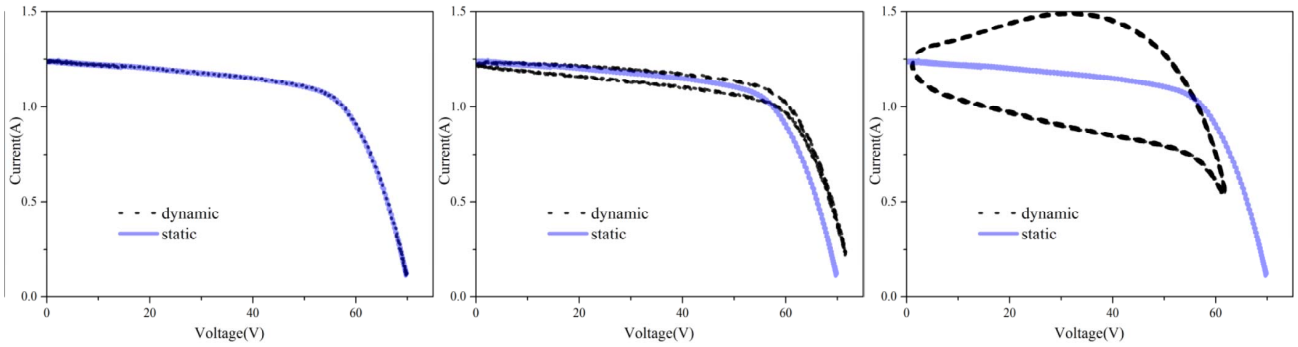

(A) 10Hz (b) 100Hz (c) 1000Hz

Fig. 1 Static and dynamic I-V characteristics of PV panels subject to different sweeping frequencies.

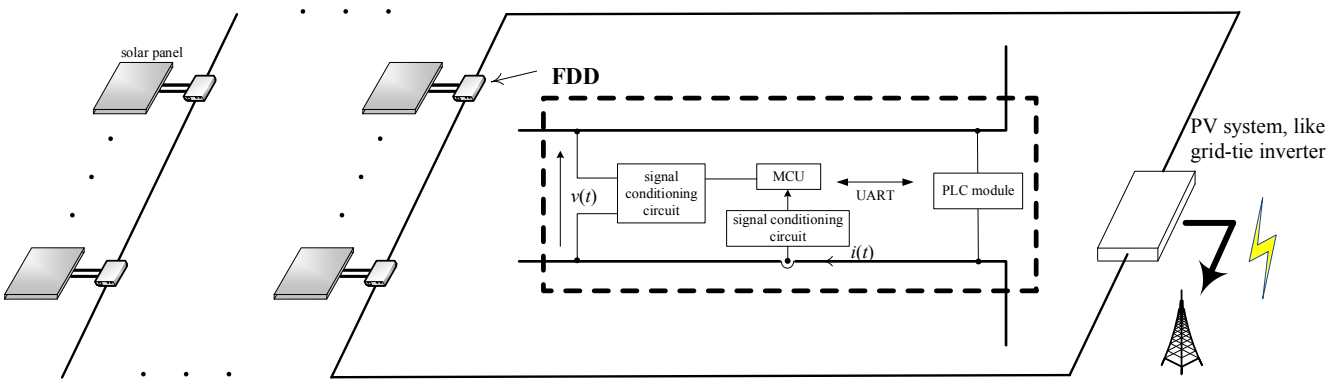

Fig. 2 Connection of the proposed fault diagnostic device to a PV system.

Fig. 2 shows a grid-tie PV inverter system. The solar panels are connected in series to form a string and each panel has a FDD mounted. Each FDD samples the terminal voltage and current of the connected panel. The FDD has a PLC module that receives commands from and sends information to the central control unit in the PV system through the power cables. The sampling time is synchronized among the FDDs. Thus, The connection is non-intrusive and does not require modification of existing infrastructure.

II. Dynamic Model of a Solar Cell

Fig. 3 shows the typical electrical model for describing the behavior of a solar cell [5]. The current source I_{ph} is the current determined by the incident light, D_{sh}, C_{sh}, and R_{sh} are used to describe the behaviour of the p-n junction, and R_s is the series resistance of the cell.

As discussed in [10] and [14], a solar panel can be modeled by the electrical model similar to the one shown in Fig. 3, except that the parameters are modified by considering the number of cells connected in series or parallel. Such

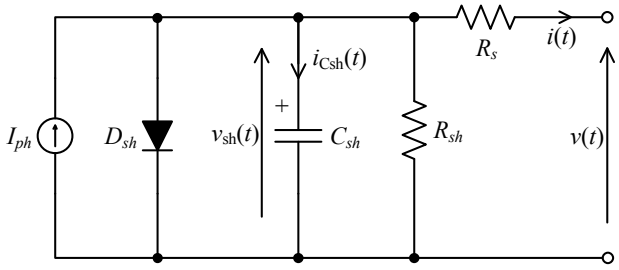

Fig. 3 Electrical model for describing the behavior of a solar cell.

aggregated parameters are identified by the algorithm described in this paper.

Mathematically,

$$i_D(v_{sh}) = I_o\,(e^{\frac{v_{sh}}{v_T}} - 1) \tag{1}$$

where I_o is the reverse saturation current of the diode, v_{sh} is the voltage across C_{sh}, and $v_T = n_{id}\,k\,T\,/\,q$, in which n_{id} is ideality factor, q is the electron charge, k is the Boltzmann constant, and T is the temperature of the p-n junction in Kelvin.

The current through C_{sh} and the rate of change of v_{sh} are

$$i_{Csh}(v_{sh}, v) = I_{ph} - i_D(v_{sh}) - \frac{v_{sh}}{R_{sh}} - \frac{v_{sh} - v}{R_s} \quad (2)$$

$$\frac{d\,v_{sh}}{d\,t}(v_{sh}, v) = \frac{1}{C_{sh}}[I_{ph} - i_D(v_{sh}) - \frac{v_{sh}}{R_{sh}} - \frac{v_{sh} - v}{R_s}] \quad (3)$$

Fig. 4 shows the change of the I-V characteristic of a solar panel with the value of C_{sh}. The sweeping frequency is 1kHz. The discrepancy between the static and dynamic I-V characteristics increases as the value of C_{sh} increases. Table I tabulates the values of the parameters used in the analysis. Fig. 1 gives the change of the I-V characteristic with the sweeping frequency using the same set of parameters.

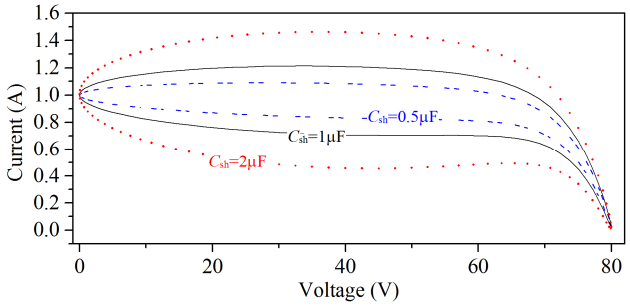

Fig. 4 IV-characteristics with different values of C_{sh}.

TABLE I – PARAMETERS USED IN THE ANALYSIS

Parameter	Value	Parameter	Value
R_s (Ω)	1	I_o (A)	1 x 10^{-7}
R_{sh} (Ω)	1000	v_T (V)	5
C_{sh} (μF)	{0.5, 1, 2}	I_{ph} (A)	1

III. MODIFIED PSO FOR PARAMETER ESTIMATION

Fig. 5 shows the mechanism of determining the intrinsic parameters of the solar panel, based on the sampled panel voltage and current information. It consists of two main parts: 1) panel current estimator, and 2) modified-PSO (MPSO) engine. The interface between these two parts is a set of the intrinsic parameters P, defined as

$$P = \{I_{ph}, I_o, v_T, R_{sh}, C_{sh}, R_s\} \quad (4)$$

The panel current estimator is used to predict the time series of the panel current, based on a series of the sampled panel voltages and the set of parameters provided by the MPSO engine. The MPSO engine is used to estimate the set of parameters by minimizing the error between a series of the actual and predicted panel currents. The operations of the two parts are described as follows.

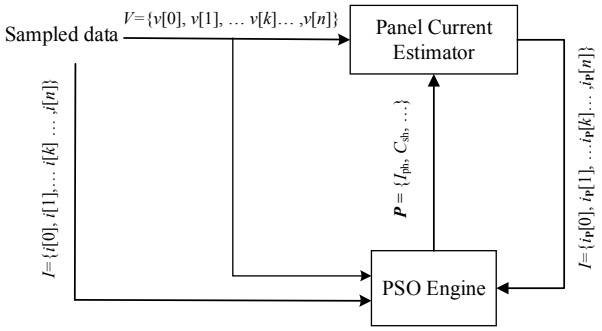

Fig. 5 Mechanism of determining the intrinsic parameters.

A. Panel Current Estimator

Let V and I be the time series of the measured panel voltage and current, respectively,

$$V = \{v[0], \quad v[1], \quad \ldots \quad v[k], \quad \ldots \quad v[N]\} \quad (5)$$

$$I = \{i[0], \quad i[1], \quad \ldots \quad i[k], \quad \ldots \quad i[N]\} \quad (6)$$

The time series of the voltage across C_{sh} , V_{sh}, is

$$V_{sh} = \{v_{sh}[0], \quad v_{sh}[1], \quad \ldots \quad v_{sh}[k], \quad \ldots \quad v_{sh}[N]\} \quad (7)$$

Let the time series of the predicted panel current be I_p,

$$I_p = \{i_p[0], \quad i_p[1], \quad \ldots \quad i_p[k], \quad \ldots \quad i_p[N]\} \quad (8)$$

The steps of determining $i_p[k]$ are listed as follows:

Step 1) – Assume that the current through C_{sh} is zero. Determine $v_{sh}[0]$ by using (1) and (3) that

$$I_o(e^{\frac{v_{sh}[0]}{v_T}} - 1) + \frac{v_{sh}[0]}{R_{sh}} + \frac{v_{sh}[0] - v[0]}{R_s} = I_{ph} \quad (9)$$

Step 2) – Calculate $i_p[k]$ with the equation

$$i_p[k] = \frac{v_{sh}[k] - v[k]}{R_s} \quad (10)$$

Step 3) – Calculate $v_{sh}[k+1]$ by solving the following trapezoidal equation with Newton's method,

$$v_{sh}[k+1] - v_{sh}[k] = \frac{h}{2}[\frac{d\,v_{sh}}{\mathrm{d}\,t}(v_{sh}[k], v[k]) + \frac{d\,v_{sh}}{d\,t}(v_{sh}[k+1], v[k+1])] \quad (11)$$

where h is the sampling time interval.

The derivatives on the right-hand-side of (11) are obtained by using (3).

Step 4) – Increase k by 1.
Step 5) – Repeat Step 2) through step 4) until $k = N$.

B. Modified PSO Engine

The MPSO engine is used to estimate the parameters of the solar panel by minimizing the objective function that measures the deviation of the predicted and measured panel currents. The objection function, MPSO algorithm, and learning factor are given as follows.

1. The Objective Function

The MPSO is used to perform the following minimization problem, so that the best set of parameters P_0 for P in (4) is determined,

$$P_0 = \arg\min_{P} f_{obj}(P), \tag{12}$$

where $f_{obj}(P)$ is the objective function.

$f_{obj}(P)$ is estimated by summing the square error of the measured and predicted panel currents in (6) and (8), respectively, over a period of time. It is defined as

$$f_{obj}(P) = \frac{1}{N_2 - N_1 + 1} \sum_{k=N_1}^{N_2} (i_p[k] - i[k])^2 \tag{13}$$

where N_1 and N_2 are the starting and ending samples, respectively, of the series in calculating $f_{obj}(P)$, $i[k]$ is the k-th sample in I defined in (6), and $i_p[k]$ is the k-th sample in I_p defined in (8).

Samples before N_1 are ignored as the initial voltage on C_{sh} is an unknown. It will have little effect on the output current after a few iterations.

B. MPSO Algorithm

Parameter estimation is conducted by minimizing the objective function defined in (13) with a modified version of PSO [15, 16]. Fig. 6 shows the flowchart of the MPSO. Let the population size of the candidate parameter sets used in each optimization generation be M. Each candidate parameter set, namely particle, holds its position P_i, where i = 1, 2, …, M, and is associated with its velocity V_i. The particle velocity V_i in the g-th optimization generation, $V_i^{(g)}$, is calculated by using the following formula [15],

$$\begin{aligned} V_i^{(g)} = w^{(g-1)} V_i^{(g-1)} &+ 2\, r_{1,i}^{(g-1)} [P_G - P_i^{(g-1)}] \\ &+ 2\, r_{2,i}^{(g-1)} [P_{H,i}^{(g-1)} - P_i^{(g-1)}] \end{aligned} \tag{14}$$

where $V_i^{(g-1)}$ is the particle velocity of the i-th particle in the (g-1)-th generation, P_G is the globally-best particle so far in the optimization, $P_i^{(g-1)}$ holds the position of the i-th particle in the (g-1)-th generation, $P_{H,i}^{(g-1)}$ holds the individual best position

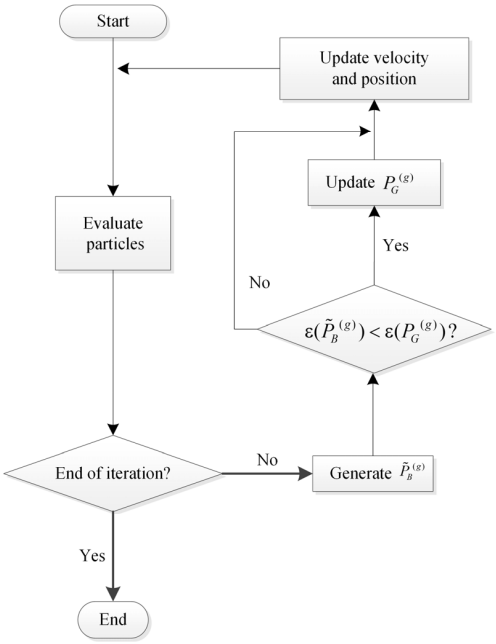

Fig. 6 Flowchart of the MPSO engine.

of the i-th particle so far, $w^{(g-1)} \in (0, 1)$ is the learning factor determined by the position of the particles and its expression is given in the next section, and $r_{1,i}^{(g-1)}$ and $r_{2,i}^{(g-1)}$ are randomly generated weighting factors distributed uniformly between 0 and 1.

In (14), $P_{H,i}^{(g-1)}$ is selected by using the following criterion,

$$P_{H,i}^{(g-1)} = \begin{cases} P_i^{(g-1)} & \text{if } f_{\text{obj}}(P_i^{(g-1)}) < f_{\text{obj}}(P_{H,i}^{(g-2)}) \\ P_{H,i}^{(g-2)} & \text{else} \end{cases} \tag{15}$$

while $P_G^{(g-1)}$ is selected by using the following criterion,

$$P_G^{(g-1)} = \arg\min_{P_{H,i}^{(g-1)}} f_{\text{obj}}(P_{H,i}^{(g-1)}), \text{ for } i = 1, 2, ..., M. \tag{16}$$

Based on (14), the particles are updated by using the following formula

$$P_i^{(g)} = P_i^{(g-1)} + V_i^{(g)} \tag{17}$$

The particles are not allowed to exceed the searching boundaries, so the velocities of the particles who reach the boundaries will be returned. To avoid the particles trapping into local optima, a perturbation technique is applied. The technique is described as follows.

Before updating particles with (17), a new particle $\tilde{P}_B^{(g)}$ is formed by mutating $P_G^{(g)}$ using a random perturbation $\delta p^{(g)}$,

$$\tilde{P}_B^{(g)} = P_G^{(g)} + \delta p^{(g)} \tag{18}$$

If $f_{\text{obj}}(\tilde{P}_B^{(g)}) < f_{\text{obj}}(P_G^{(g)})$, i.e., particle $\tilde{P}_B^{(g)}$ is better than $P_G^{(g)}$, the best one in $\{P_G^{(g)} + \delta p^{(g)}, P_G^{(g)} + 2\delta p^{(g)}, P_G^{(g)} + 4\delta p^{(g)}, \ldots, P_G^{(g)} + 2^j \delta p^{(g)}\}$ will be substituted for $P_G^{(g)}$, where $P_G^{(g)} + 2^j \delta p^{(g)}$ is within the searching boundaries and $P_G^{(g)} + 2^{j+1} \delta p^{(g)}$,

$$P_G^{(g)} = \arg\min_p f_{\text{obj}}(p), \text{ subject to: } p = P_G^{(g)} + 2^r \delta p^{(g)} \quad (19)$$

where $r = 0, 1, 2, \ldots, j$.

With the help of Fig. 6, a brief description of the estimation steps is listed as follows,

Step 1) - All M particles are initialized randomly.

Step 2) - All particles are evaluated by (13).

Step 3) - A new particle is generated by mutating the best particle using (18).

Step 4) - The best particle in the swarm will be replaced by the best one in (19) if the condition is met.

Step 5) - The velocities of all particles are calculated by (14), and positions are updated by (17).

Step 6) - The procedure is repeated from *Step 2)* for the next generation.

The procedures are simple and do not utilize much computational resources.

C. Calculation of the Learning Factor w

Detailed derivation of the learning factor w in each generation is given in [16]. The procedures are described as follows:

Step 1 - Calculate the "mean distance" of each particle P_i to all the other particles

$$d_i = \frac{1}{N-1} \sum_{j=1,\, j\neq i}^{N} d_{euc}(P_i, P_j) \quad (20)$$

where N is the number of particles in the swarm and $d_{euc}(P_i, P_j)$ is the normalized Euclidian distance from particle P_j to particle P_i.

The formula of $d_{euc}(P_i, P_j)$ is

$$d_{euc}(P_i, P_j) = \sqrt{\sum_{k=1}^{D} \left(\frac{P_{i,k} - P_{j,k}}{U_k - L_k}\right)^2} \quad (21)$$

where D is the dimension of particles, $P_{i,k}$ is the k-th scalar quantity in P_i, and U_k and L_k are the upper bound and lower bound in the k-th dimension of the search range, respectively.

Step 2 - Denote the "mean distance" of the globally best particle as d_g and find out the maximum and minimum "mean distance", $d_{\max}$ and $d_{\min}$, respectively, among the swarm.

Then, compute an "evolutionary factor" defined as

$$f = \frac{d_g - d_{\min}}{d_{\max} - d_{\min}} \quad (22)$$

Thus, $f \in [0, 1]$.

Step 3 – The learning factor w is calculated by using the following sigmoid function

$$w(f) = \frac{1}{1 + 1.5e^{-2.6f}} \quad (23)$$

The evolutionary factor reflects the diversity of particles, and affects the learning factor that controls the converging rate of the swarm.

IV. Verification of the Algorithm

The accuracy of the proposed algorithm is tested by using a series of simulated voltage and current information using the parameters tabulated in Table I. The value of C_{sh} used in the simulation is 1μF. The sweeping frequency used is 1kHz. The search range of the parameters is given in Table II and the controlling factors for the MPSO are given in Table III.

TABLE II –SEARCH RANGE OF THE PARAMETERS

Parameter	Min. value	Max. value
I_{ph} (A)	0.1	2
I_o (A)	1×10^{-9}	1×10^{-3}
v_T (V)	0.1	1000
R_{sh} (Ω)	100	10000
C_{sh} (F)	1×10^{-7}	1×10^{-5}
R_s (Ω)	0.1	10

TABLE III – CONTROLLING FACTORS

Factor	Value	Note
M	25	Population of the swarm
N_{itr}	20000	Number of iterations
N_1	100	Start of calculating the objective function
N_2	300	End of calculating of the objective function
α	1×10^{-5}	Accuracy taken in the Newton's method

Table IV shows the performance statistics of the proposed parameter estimation algorithm in 50 independent executions with different initial particles. It can be observed that the results are very close to the actual values used in the simulation. Moreover, the standard deviation is negligible, implying that every run would produce identical results for a given set of data. Therefore, the algorithm could be reliably applied to parametric estimation for solar panels.

Fig. 7 shows the value of the objective function in 20000 generations. The estimation process converges after 10000 generations.

TABLE IV - PERFORMANCE STATISTICS

Parameter	Original Value	Mean	Standard Deviation
I_{ph} (A)	1	0.9995	4.77×10^{-9}
I_0 (A)	1×10^{-7}	9.091×10^{-8}	1.56×10^{-13}
v_T (V)	5	4.971	5.24×10^{-7}
R_{sh} (Ω)	1000	1007.2	2.12×10^{-4}
C_{sh} (F)	1×10^{-6}	1.004×10^{-6}	9.34×10^{-15}
R_s (Ω)	1	1.053	5.64×10^{-7}

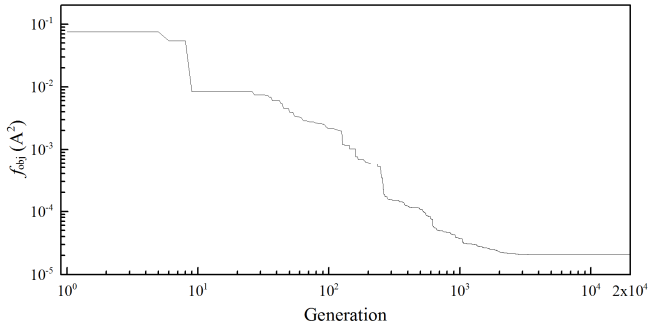

Fig. 7 Value of the objective function versus generation.

V. EXPERIMENTAL VERIFICATION

An experimental system shown in Fig. 8 has been constructed. It consists of a chamber with controllable irradiance. Four panels, P1 ~ P4, are placed in the chamber. Two of them, P1 and P4, are healthy and the other two, P2 and P3, have different degrees of damage. Fig. 9 shows the cracks on P2 and P3. P3 has more severe damage. A prototype fault diagnostic device with a Cortex M4 microcontroller unit, signal conditioning circuit for sensing the panel voltage and current, and a PLC module, has been built. The sampling frequency is 100kHz. The output of the panel is connected to an electronic load HP6050A to emulate the input of a MPP tracker in a PV system. A computer is used to control the impedance of the electronic load and communicate with the prototype device through the PLC. The test is conducted in the following steps:

1. The irradiance of the chamber is controlled.
2. The computer informs the device of the upcoming operation.
3. The panel voltage is swept by using the electronic load.
4. The device collects all voltage and current information and starts the estimation algorithm.
5. The device sends the results back to the computer.

All four panels were tested in two situations: (a) the lights were just turned on and the panels were still cool; (b) the lights had been turned on for two minutes, and the panels were heated up. The voltage and current were first acquired by 12-bit ADCs at a sampling rate of 1.4 MS/s, and then compressed to 100kS/s by averaging. The frequency of the excitation signal generated by computer was 1kHz. Thus, only several

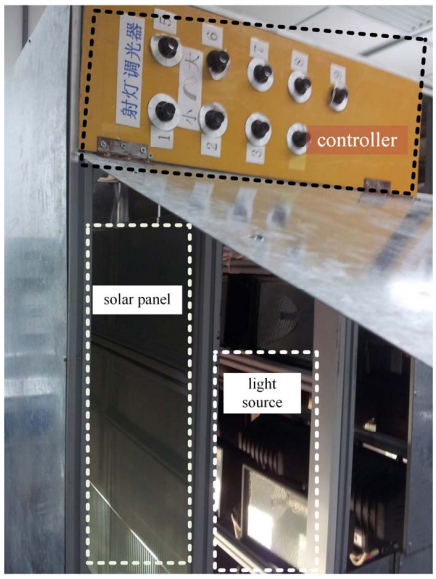

Fig. 8 Experimental setup.

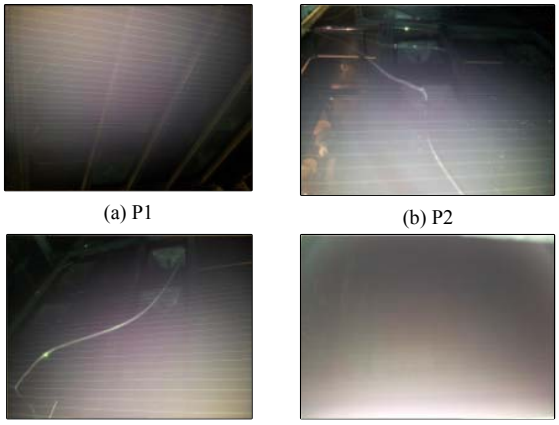
(a) P1 (b) P2 (c) P3 (d) P4
Fig. 9 Four solar panels used in the experiment.

milliseconds of excitation are required. The amount of time to perform PSO for each case was nearly an hour on the MCU, and about one or two minutes on a dual-core computer by comparison.

Fig. 10 shows the measured and estimated panel voltage and panel current waveforms of the panels P1 (without crack) and P2 (with cracks) under low- and high-temperature operations. The estimated waveforms are obtained by using the model described in Section II and the panel current estimator described in Section III. The estimated current waveforms can match the experimental results well for the considered time interval. Fig. 11 shows the value of the objection function versus the generation. It can be observed that the results converge to a satisfactory level after 20000 generations.

TABLE VI – RESULTS OF PARAMETER ESTIMATION FROM MEASURED DATA

Parameter	Low temperature				High temperature			
	P1	P2 (cracked)	P3 (cracked)	P4	P1	P2 (cracked)	P3 (cracked)	P4
I_{ph} (A)	1.10	0.561	0.430	1.11	1.18	0.602	0.454	1.21
I_o (A)	3.14×10^{-6}	6.09×10^{-8}	6.59×10^{-9}	1.55×10^{-7}	4.13×10^{-6}	7.09×10^{-8}	1.80×10^{-8}	1.40×10^{-7}
v_T (V)	7.25	5.57	5.22	5.86	6.95	5.26	5.23	5.47
R_{sh} (Ω)	449	408	655	493	427	369	587	442
C_{sh} (μF)	0.293	0.220	0.153	0.238	0.320	0.240	0.157	0.262
R_s (Ω)	1.74	2.43	5.10	0.95	1.86	2.60	4.82	1.44

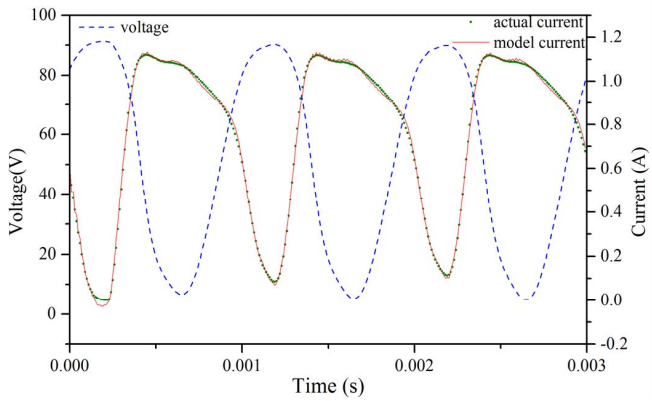

(a) P1, under low temperature.

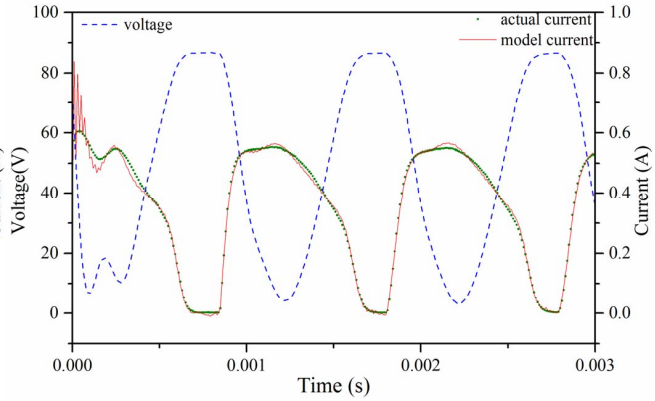

(a) P2, under low temperature.

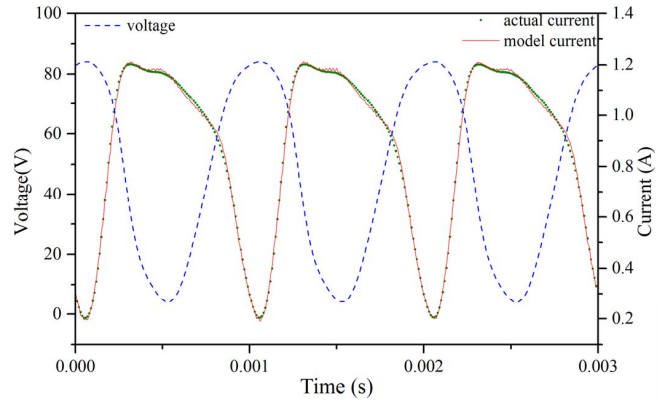

(a) P1, under high temperature.

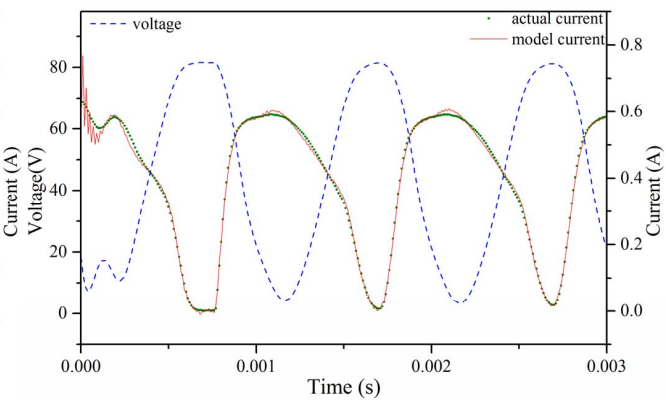

(a) P2, under high temperature.

Fig. 10 Measured and estimated panel voltage and panel current waveforms of the panels P1 and P2.

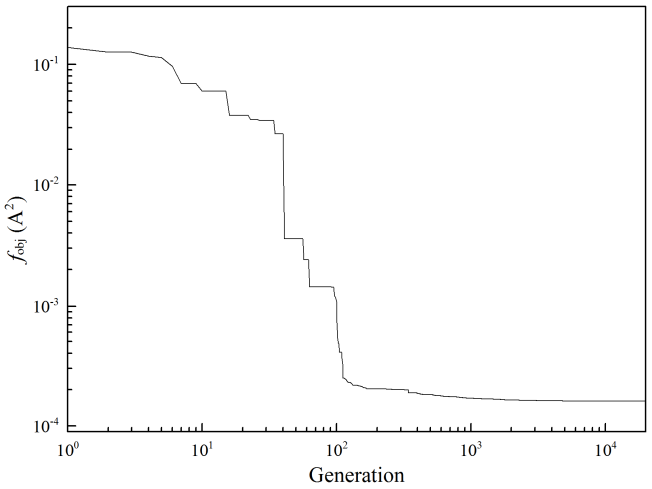

Fig. 11 Value of the objective function versus generation.

Table VI shows the results of the parameter estimation when the panels are operated under high- and low-temperature. The following observations are drawn:

- The magnitudes of I_{ph} of the cracked panels are smaller than that of the healthy panels. However, it cannot be treated as an indicator for fault analysis because I_{ph} is also affected by the irradiance. Under the partial shading condition, I_{ph} could be varied significantly within the same panel string.
- The range of I_o is mostly diverse. Cracked panels tend to have smaller I_o in the experiments.
- The value of v_T does not vary too much in all cases.
- The value of R_{sh} varies among all cases, even though there is tendency that the value of R_{sh} of P3 is increased. Such value cannot be treated as an indication, as its value is affected by how the panel is damaged.
- The value of C_{sh} is reduced and the value of R_s is increased in the cracked panels.

The drift of the values of C_{sh} and R_s can give indications for fault diagnosis.

VI. Conclusions

This paper presents a fault diagnostic device for PV panels. Detailed implementation of the device and its performance have been given. Experiments reveal that proposed device can provide operators with a fault diagnosis tool without interruption of power generation. Furthermore, the merits lie in its modularity, scalability, and remote sensing capability without modifying existing infrastructure.

Acknowledgment

This work was supported by a grant from the Innovation and Technology Fund of the Hong Kong Special Administrative Region, China, through Project (GHP/017/12SZ), National High-Technology Research and Development Program ("863" Program) of China under Grant 2013AA01A212, in part by the NSFC for Distinguished Young Scholars 61125205, in part by the NSFC No. 61332002, No. 61300044, and No. 61070004.

References

[1] O. Shekoofa and M. Taherbaneh, "Modelling of Silicon Solar Panel by MATLAB/Simulink and Evaluating the Importance of Its Parameters in a Space Application," *2007 3rd Int. Conf. Recent Adv. Sp. Technol.*, pp. 719–724, Jun. 2007.

[2] E. M. D. S. Brito, a. F. Cupertino, L. P. Carlette, D. O. Filho, H. a. Pereira, and P. F. Ribeiro, "Comparison of solar panel models for grid integrations studies," *2012 10th IEEE/IAS Int. Conf. Ind. Appl.*, pp. 1–8, Nov. 2012.

[3] H. Wei and J. Cong, "Extracting solar cell model parameters based on chaos particle swarm algorithm," in *2011 International Conference on Electric Information and Control Engineering*, 2011, pp. 398–402.

[4] A. Reza Reisi, M. Hassan Moradi, and S. Jamasb, "Classification and comparison of maximum power point tracking techniques for photovoltaic system: A review," *Renew. Sustain. Energy Rev.*, vol. 19, pp. 433–443, Mar. 2013.

[5] P. Suskis and I. Galkin, "Enhanced photovoltaic panel model for MATLAB-simulink environment considering solar cell junction capacitance," in *IECON 2013 - 39th Annual Conference of the IEEE Industrial Electronics Society*, 2013, pp. 1613–1618.

[6] K. Ishaque and Z. Salam, "A Deterministic Particle Swarm Optimization Maximum Power Point Tracker for Photovoltaic System Under Partial Shading Condition," *IEEE Trans. Ind. Electron.*, vol. 60, no. 8, pp. 3195–3206, 2013.

[7] M. Miyatake, M. Veerachary, F. Toriumi, N. Fujii, and H. Ko, "Maximum Power Point Tracking of Multiple Photovoltaic Arrays: A PSO Approach," *IEEE Trans. Aerosp. Electron. Syst.*, vol. 47, no. 1, pp. 367–380, Jan. 2011.

[8] K. L. Lian, J. H. Jhang, and I. S. Tian, "A Maximum Power Point Tracking Method Based on Perturb-and-Observe Combined With Particle Swarm Optimization," *IEEE J. Photovoltaics*, vol. 4, no. 2, pp. 626–633, Mar. 2014.

[9] Y. Zhao, L. Yang, B. Lehman, J.-F. de Palma, J. Mosesian, and R. Lyons, "Decision tree-based fault detection and classification in solar photovoltaic arrays," in *2012 Twenty-Seventh Annual IEEE Applied Power Electronics Conference and Exposition (APEC)*, 2012, pp. 93–99.

[10] J. Soon and K. Low, "Photovoltaic model identification using particle swarm optimization with inverse barrier constraint," *Power Electron. IEEE Trans.*, vol. 27, no. 9, pp. 3975–3983, 2012.

[11] F. Yu, P. Zhang, W. Xiao, and P. Choudhury, "Communication systems for grid integration of renewable energy resources," *Network, IEEE*, no. October, pp. 22–29, 2011.

[12] E. Roman, R. Alonso, P. Ibanez, S. Elorduizapatarietxe, and D. Goitia, "Intelligent PV Module for Grid-Connected PV Systems," *IEEE Trans. Ind. Electron.*, vol. 53, no. 4, pp. 1066–1073, Jun. 2006.

[13] Y. Son, T. Pulkkinen, K. Moon, and C. Kim, "Home energy management system based on power line communication," *IEEE Trans. Consum. Electron.*, vol. 56, no. 3, pp. 1380–1386, Aug. 2010.

[14] J. M. Blanes, F. J. Toledo, S. Montero, and A. Garrigós, "In-Site Real-Time Photovoltaic I–V Curves and Maximum Power Point Estimator," *IEEE Trans. Power Electron.*, vol. 28, no. 3, pp. 1234–1240, Mar. 2013.

[15] J. Kennedy and R. Eberhart, "Particle swarm optimization," in *Proceedings of ICNN'95, International Conference on Neural Networks*, 1995, vol. 4, pp. 1942–1948.

[16] Z. H. Zhan, J. Zhang, Y. Li, and H. S. H. Chung, "Adaptive Particle Swarm Optimization," *IEEE Trans. Syst. Man Cybern. Part B-Cybernetics*, vol. 39, no. 6, pp. 1362–1381, 2009.